

# Terahertz spectroscopic signature of the charge density wave in the spin-ladder compound, $\text{Sr}_{14}\text{Cu}_{24}\text{O}_{41}$

Soumitra Hazra<sup>1</sup>, Rabindranath Bag<sup>2</sup>, Surjeet Singh<sup>2</sup>   
and Rajeev N Kini<sup>1,3</sup> 

<sup>1</sup> Indian Institute of Science Education and Research Thiruvananthapuram (IISER-TVM), Maruthamala P.O. Vithura, Kerala 695551, India

<sup>2</sup> Indian Institute of Science Education and Research Pune (IISER Pune), Dr Homi Bhabha Road, Pashan, Pune, 411008, India

E-mail: [rajeevkini@iisertvm.ac.in](mailto:rajeevkini@iisertvm.ac.in)

Received 27 January 2020, revised 21 February 2020

Accepted for publication 10 March 2020

Published 9 April 2020



## Abstract

We provide spectroscopic evidence for the charge density wave (CDW) phason mode at  $\approx 0.93$  THz in the two-leg, spin-1/2 ladders of  $\text{Sr}_{14}\text{Cu}_{24}\text{O}_{41}$  using terahertz time-domain spectroscopy. We find that annealing in an oxygen atmosphere or doping with a low concentration of Co ( $\lesssim 1\%$ ) does not affect the CDW phason mode. However, Co doping at higher concentrations (10%), wherein the Co enters the ladder layers, destabilizes the CDW. We believe that the suppression of the CDW phase is due to an increase in intraladder overlap integrals through the shrinkage of interplane distance upon Co doping.

Keywords: strongly correlated systems, charge density wave, THz spectroscopy, spin-ladder compounds

 Supplementary material for this article is available [online](#)

(Some figures may appear in colour only in the online journal)

## 1. Introduction

Antiferromagnetic spin-1/2, two-leg ladders show intriguing magnetic and superconducting properties that have continued to attract considerable interest. The spin-1/2 ladders, which exhibit a spin-singlet ground state with a gapped excitation spectrum, were theoretically predicted to show superconductivity upon hole-doping [1]. This was subsequently confirmed in the high-pressure experiments on the Ca-doped  $\text{Sr}_{14}\text{Cu}_{24}\text{O}_{41}$  (SCO) system, which is generally regarded as an ideal two-leg ladder system [2]. The crystal structure of SCO consists of alternating  $\text{CuO}_2$  chains and  $\text{Cu}_2\text{O}_3$  ladders layers stacked along the  $b$ -axis, separated by Sr atoms. SCO is intrinsically hole-doped with six holes per formula unit, and the

holes are distributed among the chains and ladders [3]. Isovalent Ca doping causes the inherent holes in the chains to transfer to the ladder substructure, which leads to superconductivity in SCO under pressure. In SCO, the superconducting ground state is believed to compete with the charge density wave (CDW) ordering [4]. The holes in the ladders crystallize through the many-body interactions favoring the formation of CDW or ‘hole crystal’ ground state which consists of paired holes periodically arranged along the length of the ladder with the commensurate wave vector  $\lambda = 5c_L$ , where  $c_L$  is the ladder lattice constant [5, 6]. However, unlike the conventional Peierls-type materials where a structural modulation accompanies CDW, the hole-crystallized phase in SCO does not involve any measurable structural variation, which led to the proposals that the strong electron–electron correlations drive this ground state [7]. Moreover, in conventional CDW materials, the CDW ordering is typically accompanied

<sup>3</sup> Author to whom any correspondence should be addressed.

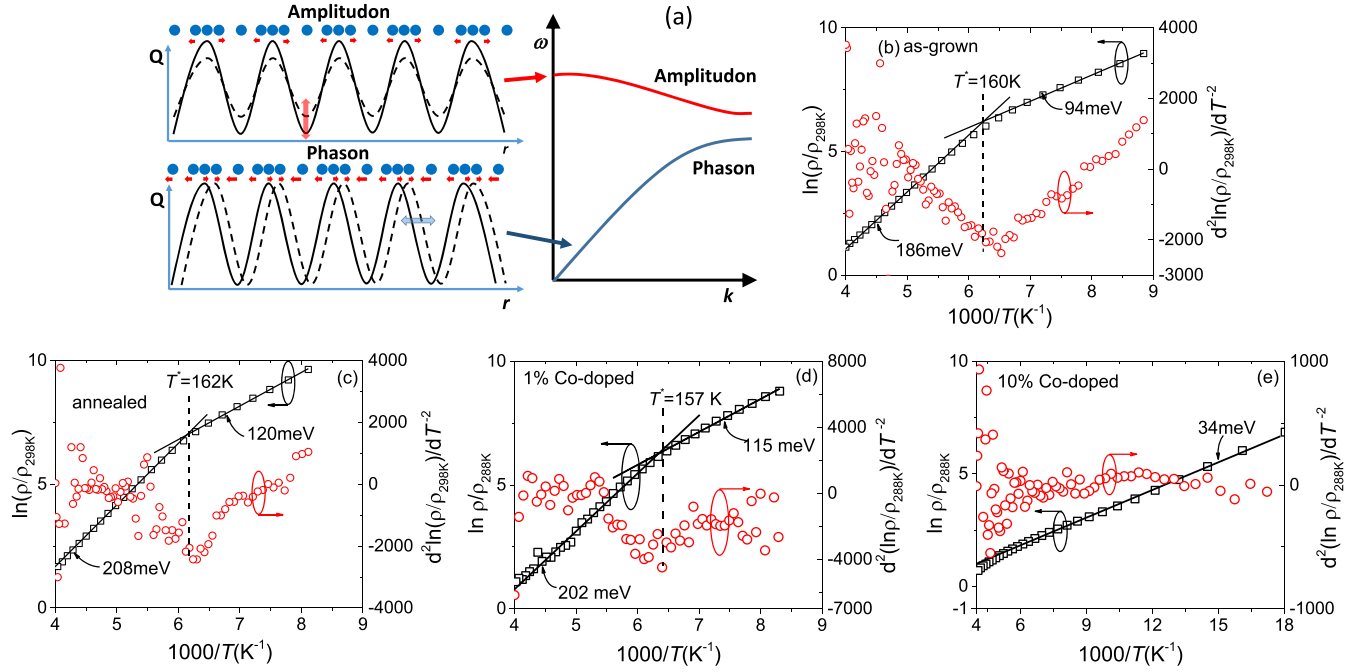


**Figure 1.** (a) Schematic illustration of the charge density wave amplitudon and phason modes along with the dispersion relation. Temperature-dependent DC resistivity of (b) as-grown SCO, (c) annealed SCO, SCO doped with (d) 1% Co and (e) 10% Co. The resistivity has been normalized to the resistivity at 298 K. The second derivative of the temperature-dependent resistivity plot is also shown.

by a metal-to-insulator transition [8], which is not the case in SCO. Electron–electron interactions in the ladder plane of SCO lead to a Mott insulator behavior above the transition temperature. Hence, an insulator-to-insulator transition occurs above the transition temperature. This underlines the complexity of hole-crystallized CDW phase in SCO [9], and therefore, it is interesting to learn more about the nature of CDW order in these compounds. The  $\text{CuO}_2$  chains and  $\text{Cu}_2\text{O}_3$  ladders layers are structurally incommensurate, which causes the flexible chain layers to buckle slightly to accommodate the rigid ladder layers. This results in an unconventional charge ordering or CDW even in the chain subsystem, which is stabilized by the strain due to the misfit ladder and chain layers [10].

The two distinct degrees of freedom associated with the CDW (amplitude and phase fluctuations) give rise to two modes, the amplitudon and phason mode, respectively. The amplitudon is Raman active, and its dispersion is like that of an optical phonon, as shown in figure 1(a). The dispersion relation for the phason is acoustic-like, as shown in figure 1(a), with  $\omega(k=0) = \Omega_p = 0$ , where  $\Omega_p$  is the frequency of the CDW phason mode, and  $k$  is the wave vector. However, in real crystals, the CDW is pinned, for example, due to disorder or impurities, and hence shifts the CDW phason mode,  $\Omega_p$  to a finite frequency in the infrared (IR) region [8]. The CDW phason mode shifts to finite frequency, also when the CDW is commensurate with the lattice, which is the case with SCO. Hence upon illumination with electromagnetic radiation, the CDW phason mode becomes visible in the complex optical spectrum. Since the CDW phason mode appears in the millimeter frequency range, THz spectroscopy has been previously used to study the CDW phason mode in manganites, nickelates, and

multiferroic materials [11–15]. In most cases, the CDW phason peak appears in the few-meV energy range, along with a broad shoulder at lower energies.

Even though experimental studies provide evidence of a CDW formation in SCO, the interpretation of the spectroscopic data associated with the pinned CDW mode is still controversial. Kitano *et al* had proposed the pinning frequency of the CDW phason mode to be 30–100 GHz ( $1\text{--}3.3\text{ cm}^{-1}$ ) using microwave measurements [16]. Gorshunov *et al* had observed a peak in the optical conductivity at 360–420 GHz ( $12\text{--}14\text{ cm}^{-1}$ ), which was assigned to the pinned CDW phason mode [17]. However, later, they reassigned this to a phonon mode and assigned another mode at 54 GHz ( $\sim 1.8\text{ cm}^{-1}$ ) to the pinned CDW mode [9]. A resonance feature at 356 GHz in the Raman response function corresponding to the phonon mode was also observed [18]. These phonon modes have also been detected in THz studies and have been attributed to the sliding motion of the chains and ladder layers [19, 20]. In this report, we provide spectroscopic evidence for a CDW phason mode at  $\approx 0.93\text{ THz}$  in SCO.

## 2. The experiment

The experiments were performed on high-quality single-crystals, which were grown using the traveling-solvent floating-zone technique. We studied three different single-crystal samples: one SCO crystal (labeled as as-grown) without doping, and two SCO crystals doped with 1% Co and 10% Co. The details of the crystal growth and characterization can be found in the reference [21]. It has been reported that annealing SCO in the  $\text{O}_2$  atmosphere breaks the dimers

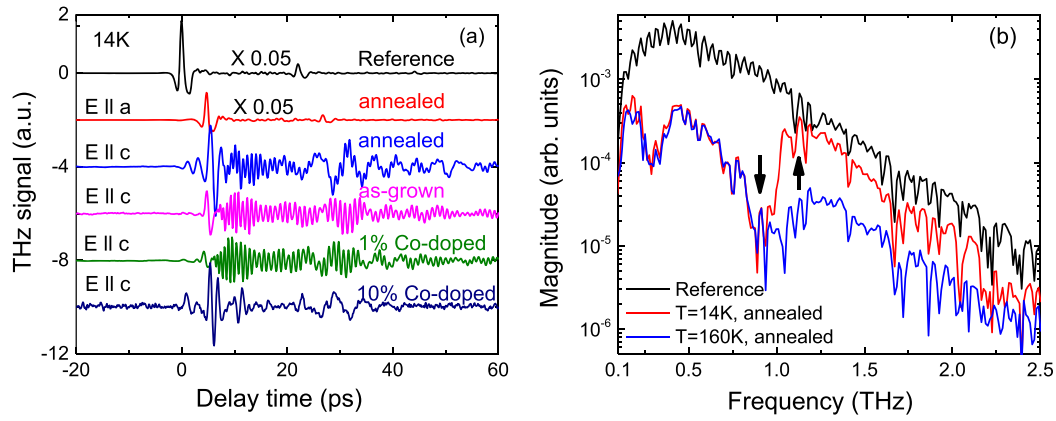


**Figure 2.** (a) Transmitted THz signal for different samples along with the reference signal. (b) The spectra of the reference THz signal and the THz signal transmitted through the annealed SCO sample at 14 K and 160 K. The downward arrow approximately indicates the position of the CDW phason mode. Because of the phason mode, the transmitted spectra has a peak near 1 THz, which is indicated by the upward arrow, which correlates with the  $\approx 1$  ps oscillations in the time domain signal.

and increases the number of free spins in the chains [22]. But, if CDW is formed in the ladders, annealing is not expected to have a significant effect on the CDW. However, annealing reduces the degree of misfit between the chains and ladders, which may, in turn, enhance the CDW spectroscopic features. Hence, the as-grown SCO crystal was later annealed in the O<sub>2</sub> atmosphere in a tubular furnace at 850 °C for 36 h and was also studied (labeled as annealed SCO). The crystals were cleaved along the  $a$ - $c$  plane into 400–700  $\mu\text{m}$  thin slices and cut into approximately  $4 \times 4$  mm pieces. For terahertz time-domain spectroscopy (THz-TDS) measurements, THz signals were generated by ultrafast ( $\approx 80$  fs) photoexcitation of a low-temperature-grown GaAs:Bi epilayer [23]. The THz signals were detected using a photoconductive antenna. THz transmittance was obtained by taking the ratio of the amplitudes of the fast Fourier transformed sample-transmitted THz signals and the reference THz signals. THz experiments were done by mounting the crystals on a sample holder with an aperture of  $\approx 3.5$  mm diameter, which was then attached to the cold finger of an ultralow-vibration optical closed-cycle cryostat. DC resistivity measurements were performed using the four-probe method. The samples were cooled to  $\approx 4$  K in a closed cycle cryostat and warmed up at a rate of  $1 \text{ K min}^{-1}$ . The DC resistivity measurements reported here were carried out during the heating cycle. The DC resistivity measurements were performed with a current of  $I = 10^{-4}$  A, and the current–voltage characteristics showed linear behavior in this current range, at both room temperature and low temperatures. Measurements were done with current with both polarities ( $+I$  and  $-I$ ) and the resistivity was obtained by averaging the two.

### 3. Results & discussion

The temperature-dependent resistivity of different samples is shown in figures 1(b)–(e). To avoid the discrepancy in resistivity, which arises from the ambiguity in the thickness of the conducting channel in these layered SCO samples, we have plotted resistivity values of each sample normalized to

its resistivity value at 298 K. As shown in figure 1(b), the normalized resistivity of the as-grown SCO crystal exhibits an Arrhenius temperature dependence with an activation energy of  $\approx 94$  meV (186 meV) below (above)  $T^* \approx 160$  K, which is consistent with earlier reports and has been accordingly attributed to the opening of the CDW gap below  $T^*$ , the change in the slope of the  $\ln(\rho)$ -vs- $1/T$  graph marks the onset of CDW and the slope below  $T^*$  indicates the CDW gap [25]. However, the determination of  $T^*$  from the experimental data is not easy since there is only a slight change in the slope of the  $\ln(\rho)$ -vs- $1/T$  graph. Hence, we obtained  $T^*$  and the slope, by fitting the experimental  $\ln(\rho)$ -vs- $1/T$  graph with a linear equation that changed the slope at  $T^*$ . The  $T^*$  thus obtained is indicated in figure 1. The second derivative of the  $\ln(\rho)$ -vs- $1/T$  graph gave a broad minimum near  $T^*$ , which further confirms the assignment of  $T^*$ .

In the case of the annealed SCO as well as the SCO sample doped with 1% Co, a  $T^*$  ( $\approx 162$  K and  $\approx 157$  K respectively) similar to the as-grown SCO, is obtained but with a higher CDW gap energy ( $\approx 120$  meV and  $\approx 115$  meV respectively), as shown in figures 1(c) and (d). The increase in the CDW gap indicates that the interaction strength leading to the formation of the CDW, which is proportional to the ratio of the CDW gap to  $T^*$ , slightly increases with annealing and Co (1%) doping. The ratio of the CDW gap to  $T^*$  in SCO is usually found to be higher than the mean-field value (3.5) due to strong 1D correlations [9]. Compared to the as-grown SCO, an increase in interaction strength was also reported in Ca (3%) doped SCO [9]. This is possibly due to off-stoichiometry in the as-grown sample [22], which reduces the interaction strength. For SCO doped with 10% Co, we obtain an activation energy of  $\approx 34$  meV. However, we do not observe any visible change in the slope near  $T^*$  [see figure 1(e)], which indicates that the transition temperature is significantly lowered or the CDW order is suppressed.

As mentioned earlier, due to the commensurate nature of the CDW or due to the pinning caused by impurities, a CDW

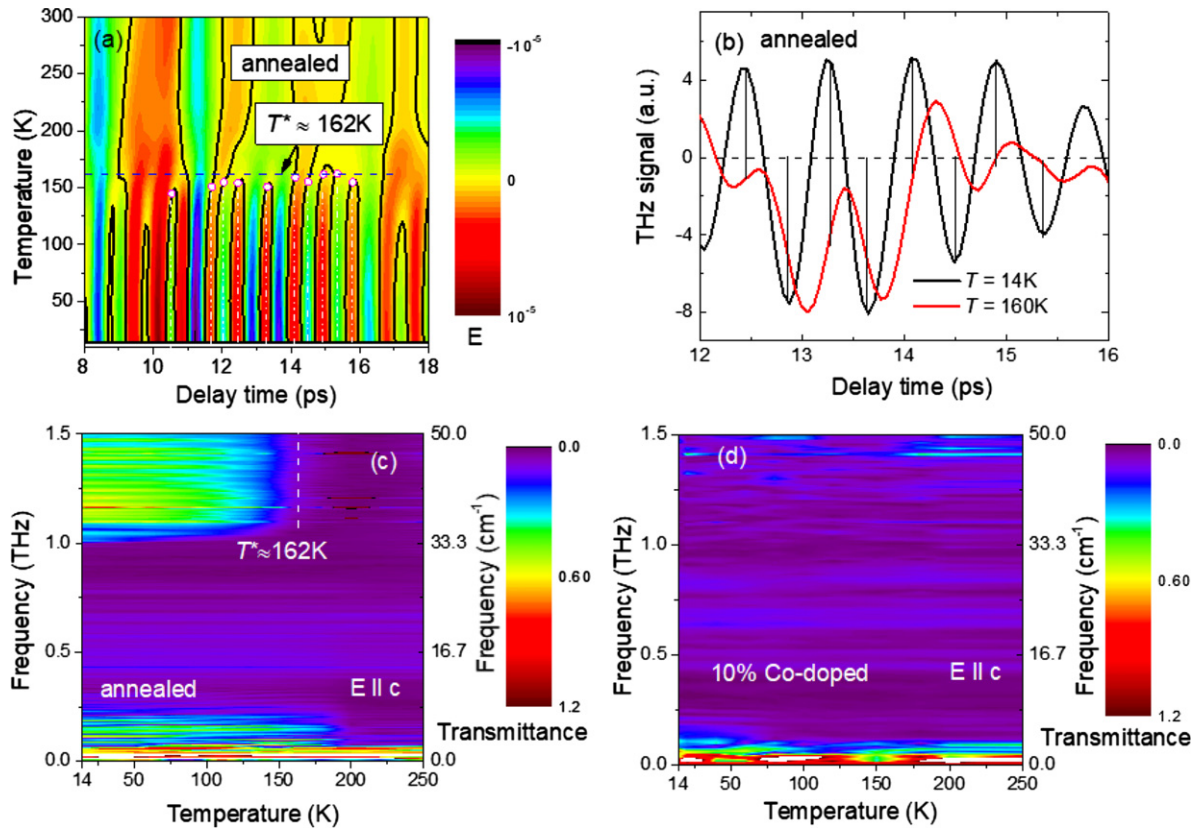


**Figure 3.** (a) Transmitted THz signal amplitude for annealed SCO crystal at different temperatures. The black contour lines are drawn for  $E = 0$ , and the white dash-dotted line indicates the  $E$  maxima. The filled circles indicate the temperature at which the oscillation extrema crossed the zero line. The dotted horizontal line indicates the  $T^*$  obtained from DC resistivity measurements. (b) Transmitted THz signal amplitude for annealed SCO crystal at 14 K and close to  $T^*$ , showing the  $\pi/2$  phase change in the signal near  $T^*$ . THz transmittance for different temperatures for the (c) annealed SCO crystal and (d) the SCO crystal doped with 10% Co.

phason mode appears, which will have signatures in the IR region. We used THz-TDS to study this CDW phason mode and its spectroscopic signatures. Figure 2(a) shows the THz signal transmitted through the as-grown, annealed, and doped SCO samples at  $T \approx 14\text{ K}$  along with the reference THz signal. The reference THz spectra, along with the spectra of the THz pulse transmitted through the annealed SCO at 14 K & 160 K, is shown in figure 2(b). For the annealed sample as well as the as-grown and SCO doped with 1% Co, at low temperatures, in the THz measurements with the THz electric field ( $E \parallel c$ ), we observed two types of oscillations in the transmitted THz signal: (i) slow oscillations with a period of  $\approx 4\text{ ps}$  and, (ii) fast oscillations with a period of  $\approx 1\text{ ps}$ . For  $E \parallel a$ , there were no oscillations in the THz signal neither for the as-grown/annealed SCO nor for the doped SCO samples, which is in agreement with the data reported earlier [19, 20]. The transmitted THz signals through the as-grown SCO and SCO doped with 1% Co were very similar to that from the annealed SCO sample. We found this to be true for all temperatures below  $T^*$ , as shown in supplementary figure S1 ([stacks.iop.org/JPhysCM/32/275601/mmedia](https://stacks.iop.org/JPhysCM/32/275601/mmedia)). The temperature dependence of the fast oscillations in annealed SCO is shown as a 2D color plot in figure 3(a). It shows that the amplitude of the fast oscillations drastically decreases near  $T^*$ . However, in the case of SCO doped with 10% Co, as shown

in figure 2(a), while the slow oscillations remain unchanged, high-frequency oscillations were highly damped even at 14 K, indicating that the CDW is suppressed. The slow oscillations arise due to the relative sliding motion of the incommensurate layers, and detailed studies concerning these oscillations have been reported earlier [19, 20]. Here, we will concentrate on the fast oscillations, which we relate to the CDW phason mode.

In figure 3(b), we show the oscillations in the transmitted THz signal through the annealed SCO at  $\approx 14\text{ K}$  and very close to  $T^*$ . It is clear from these plots that the fast oscillations undergo a phase change of  $\pi/2$  near  $T^*$  obtained from DC resistivity measurements [26]. To get a better understanding of the changes in amplitude of these oscillations, we show the temperature-dependent THz transmittance through the annealed SCO crystal in figure 3(c). As reported earlier, the transmission of THz waves in the frequency band,  $\approx 0.31\text{--}1\text{ THz}$ , is highly attenuated [19]. The high-frequency cut-off edge ( $\approx 1\text{ THz}$ ) persists up to  $T^*$ , above which the conductivity of the sample increases sharply, and THz transmission through the sample is completely blocked. THz measurements done with  $E \parallel a$  did not show any such sharp frequency cut-offs at  $\approx 1\text{ THz}$ , indicating the anisotropic nature. The as-grown SCO and SCO doped with 1% Co also exhibited similar behavior,



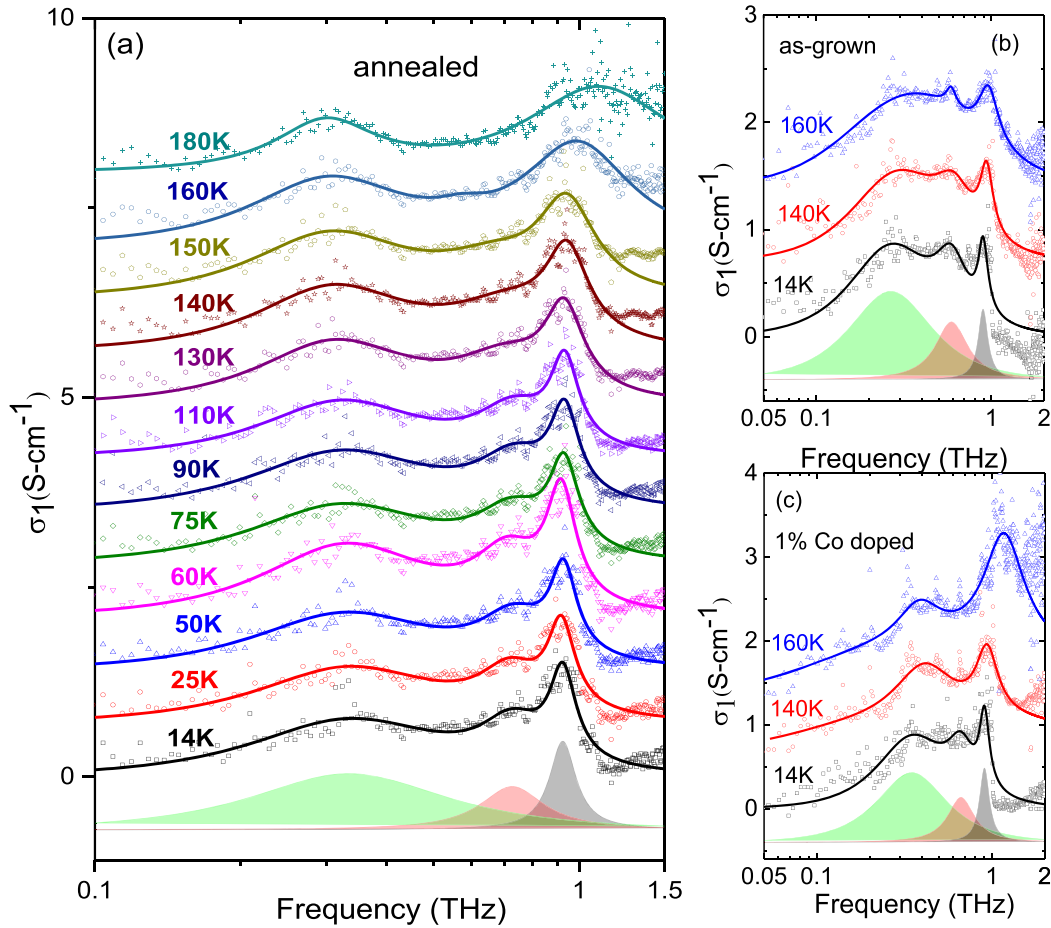


**Figure 4.** The real part of the complex optical conductivity spectrum for different temperatures for the (a) annealed SCO sample and (b) as-grown SCO sample and (c) SCO sample doped with 1% Co. The solid lines represent the fitting results to the experimental data (open symbols) using a multi-Lorentzian expression incorporating three peaks. The individual Lorentzian peaks for the 14 K data are shown as shaded peaks.

as shown in supplementary figure S1. However, temperature-dependent THz transmittance of the SCO sample doped with 10% Co did not show any of these features [see figure 3(d)].

From the above discussion, we can understand that SCO samples have an absorption mode (indicated by the downward arrow in figure 2(b)) just below 1 THz, which blocks THz transmission through the samples below 1 THz. This leads to a peak structure just above 1 THz [indicated by the upward arrow in figure 2(b)] in the transmitted spectrum, which manifests as fast oscillations with a period  $\approx 1$  ps in the THz signal transmitted through the SCO samples. Even though transmission spectra can be used to assign the different absorption modes [27, 28], transmission spectra are not conventionally used to ascribe the CDW phason mode. Instead, CDW phason modes have been identified using optical conductivity measurements in different material systems [29, 30]. We numerically estimated the complex optical conductivity spectrum using the Fourier transformed amplitude and phase of the THz pulse transmitted through the samples [11]. Figure 4(a) shows the real part of the complex THz optical conductivity at different temperatures for the annealed SCO sample. Two peak structures are observed (i) at around 0.31 THz, which was earlier assigned to the sliding phonon mode and, (ii) at about

0.93 THz, which we attribute to the CDW phason mode. To fit the peaks in the optical conductivity data, we have used the Lorentzian oscillator expression,  $\sigma_1(\omega) = \frac{\sigma_0 \omega^2 / \tau^2}{(\omega_0^2 - \omega^2)^2 + \omega^2 / \tau^2}$  where,  $\omega_0$  the peak frequency and  $\tau$  is the relaxation time. Apart from the two peaks at  $\approx 0.31$  THz and  $\approx 0.93$  THz, we find an additional peak at around  $\approx 0.65$  THz, though the origin of this is not known at this point. The peak at  $\approx 0.93$  THz is visible up to  $T^*$ . Above  $T^*$  the peak broadens and moves to higher frequencies and eventually smears into the background. As shown in figures 4(b) and (c), the similar behavior is observed for as-grown SCO and SCO doped with 1% Co.

We assign this mode, which results in the fast oscillations in the THz time-domain signal and manifested as a peak at  $\approx 0.93$  THz in the conductivity spectrum, to the CDW phason mode since (i) the onset of these fast oscillations, coincides with the CDW transition temperature,  $T^*$  obtained from DC resistivity measurements, (ii) the oscillations undergo a phase change of  $\pi/2$  near  $T^*$  in agreement with the observations in other CDW systems [26], (iii) the oscillations in the time domain and the  $\approx 0.93$  THz mode in the optical conductivity is observed only along the high conductivity  $c$ -axis consistent with the quasi-1D nature of the CDW, (iv) the oscillations and the  $\approx 0.93$  THz mode disappear on doping with Co (10%), presumably due to

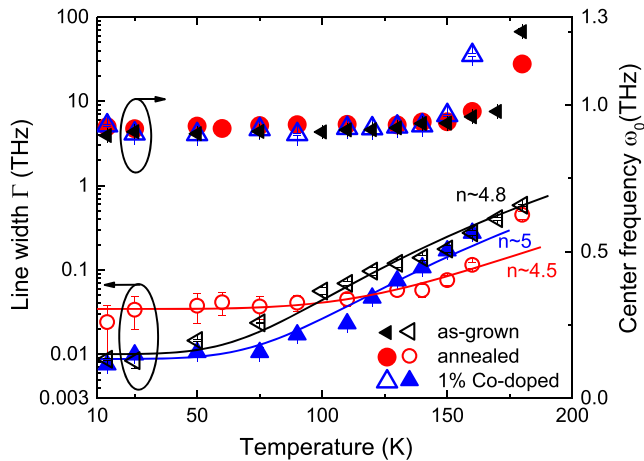


**Figure 5.** The center frequency of the CDW phason mode near 0.93 THz and its line-width obtained from the Lorentzian fitting is plotted as a function of temperature for different samples. The solid line represents fitting of the extracted linewidth (symbols) to an equation of the form,  $\Gamma = A + BT^n$  with  $n$  as indicated in the graph.

disorder leading to the loss of 1D nature of CDW and, (v) the energy of the  $\approx 0.93$  THz mode agrees well with the energy range of the CDW phason mode observed in some other well-known CDW compounds [11, 13–15]. The CDW can also give rise to an amplitudon mode, and the amplitudon mode generally produces oscillations in the reflectivity in the optical pump–probe experiments. However, pump–probe measurements on SCO have not revealed any CDW amplitudon mode [31, 32]. Also, THz and infrared spectroscopy usually probe the CDW phason mode [9, 16, 17, 33]. Hence we exclude the possibility that the peak at  $\approx 0.93$  THz in the conductivity spectra to be due to the amplitudon mode.

As shown in figure 5, we find that the peak position of the CDW phason mode does not change much with temperature below  $T^*$  and moves to higher frequencies above  $T^*$ . The width of the mode follows a  $T^n$  dependence with  $n \approx 4$ –5, which agrees well with theoretical predictions [34] and suggests that scattering due to thermal phasons or phonons is the dominant mechanism that leads to the damping of the CDW phason mode [35]. The temperature dependence of the sliding mode ( $\approx 0.25$ – $0.4$  THz) and the unknown mode ( $\approx 0.6$ – $0.75$  THz) is also shown in supplementary figure S2.

Gorshunov *et al* had suggested that the CDW develops in the chain sublattice [17], whereas other reports indicated that the CDW develops in the ladder [6, 7, 9, 25, 36]. To throw light on this issue, we discuss the data on the Co-doped SCO crystals. In a previous study, it was shown that at low doping concentration Co prefers to enter the chain sublattice. However, at doping levels higher than 3%, Co concentration in the chains saturates, and it starts doping the ladder [37]. As discussed earlier, with 1% Co doping, the signature of CDW formation is still observed. However, with 10% Co doping, the fast oscillations were strongly suppressed, see figure 2(a), since at 10% doping a good fraction of Co, in valence state +3, enters the ladders. The above discussion suggests that since the CDW mode is affected by the presence of impurities in the ladders (10% Co) and not by those in the chains (1% Co), the CDW is

formed in the ladder rather than in the chain sublattice, which supports similar conclusions drawn in several previous studies [6, 7, 9, 25, 36].

In the earlier studies, it has been shown that Ca substitution in SCO increases the intraladder overlap integrals through the shrinkage of interplane distance, which leads to the suppression of the CDW phase [25, 38]. We believe that Co substitution at  $\approx 10\%$  has a similar effect, and tends to destabilize the CDW due to the increased coupling between the chains and ladders [25, 39]. From previous studies, it is known that substitution of smaller and isovalent  $\text{Ca}^{2+}$  ion at the Sr-site or application of high pressure leads to the enhancement of ladder-chain interaction due to a decrease in the interlayer distance [38]. The reduction in the  $b$ -axis lattice parameter due to Ca-doping or due to applied pressure is approximately 0.59% per Ca or 0.73% per GPa, respectively [38]. The effect of  $\text{Co}^{3+}$  doping on the lattice parameter is also anisotropic, and the  $b$ -axis lattice parameter decreases by 0.21% per Co [21]. This is expected to enhance the chain-ladder interaction, analogous to Ca doping, and hence redistribute the holes between chain and ladder via locally formed  $\text{Cu}_{\text{ladder}} 3d$  and  $\text{O}_{\text{chain}} 2p$  hybrid orbitals [38]. The carrier localization potential in the CDW ordered state at low temperature is, therefore, expected to be partially screened due to an increase in the hole carriers in the ladder sublattice upon Co doping, analogous to the suppression of the hole-pair ordered states due to Ca-doping or applied pressure. Hence, this leads to the suppression of CDW upon doping the SCO with  $\approx 10\%$  Co.

More studies like magnetic quantum oscillations or transient grating spectroscopy are required to obtain further insights into the nature of the CDW in SCO. Since, the degree of misfit can be controlled by the annealing conditions (type of gas atmosphere, pressure, temperature and time), in future, it would be interesting to carry out detailed and systematic studies on the effect of these parameters on the CDW phase and the phason mode.

## 4. Conclusions

In conclusion, we have provided evidence for a CDW phason mode at  $\approx 0.93$  THz in SCO. Co at low concentration ( $\approx 1\%$ ) enters the chain layers in SCO and, the CDW formation is not affected. However, doping the ladders with impurities (10% Co) destabilizes the CDW, and the CDW phason mode disappears. We believe this to be due to the increased coupling between the chains and ladders caused by the shrinkage of interplane distance with Co ( $\approx 10\%$ ) doping.

## Acknowledgments

Authors thank Vaisakh for help with THz measurements.

## ORCID iDs

Surjeet Singh <https://orcid.org/0000-0001-7990-9994>  
Rajeev N Kini <https://orcid.org/0000-0002-3305-9346>

## References

- [1] Dagotto E, Riera J and Scalapino D 1992 Superconductivity in ladders and coupled planes *Phys. Rev. B* **45** 5744
- [2] Uehara M, Nagata T, Akimitsu J, Takahashi H, Mōri N and Kinoshita K 1996 Superconductivity in the ladder material  $\text{Sr}_{0.4}\text{Ca}_{13.6}\text{Cu}_{24}\text{O}_{41.84}$  *J. Phys. Soc. Japan* **65** 2764–7
- [3] Nücker N, Merz M, Kuntscher C A, Gerhold S, Schuppler S, Neudert R *et al* 2000 Hole distribution in (Sr, Ca, Y, La) $_{14}\text{Cu}_{24}\text{O}_{41}$  ladder compounds studied by x-ray absorption spectroscopy *Phys. Rev. B* **62** 14384
- [4] Elbio D 1999 Experiments on ladders reveal a complex interplay between a spin-gapped normal state and superconductivity *Rep. Prog. Phys.* **62** 1525
- [5] Rusydi A, Berciu M, Abbamonte P, Smadici S, Eisaki H, Fujimaki Y *et al* 2007 Relationship between hole density and charge-ordering wave vector in  $\text{Sr}_{14-x}\text{Ca}_x\text{Cu}_{24}\text{O}_{41}$  *Phys. Rev. B* **75** 104510
- [6] Rusydi A, Ku W, Schulz B, Rauer R, Mahns I, Qi D *et al* 2010 Experimental observation of the crystallization of a paired holon state *Phys. Rev. Lett.* **105** 026402
- [7] Abbamonte P, Blumberg G, Rusydi A, Gozar A and Evans P G 2004 Crystallization of charge holes in the spin ladder of  $\text{Sr}_{14}\text{Cu}_{24}\text{O}_{41}$  *Nature* **431** 1078
- [8] Gruener G 1988 The dynamics of charge-density waves *Rev. Mod. Phys.* **60** 1129–81
- [9] Vuletić T, Korin-Hamzić B, Tomić S, Gorshunov B, Haas P, Rößm T *et al* 2003 Suppression of the charge-density-wave state in  $\text{Sr}_{14}\text{Cu}_{24}\text{O}_{41}$  by calcium doping *Phys. Rev. Lett.* **90** 257002
- [10] Rusydi A, Abbamonte P, Eisaki H, Fujimaki Y, Smadici S, Motoyama N *et al* 2008 Strain amplification of the 4kF chain instability in  $\text{Sr}_{14}\text{Cu}_{24}\text{O}_{41}$  *Phys. Rev. Lett.* **100** 036403
- [11] Kida N and Tonouchi M 2002 Spectroscopic evidence for a charge-density-wave condensate in a charge-ordered manganite: observation of a collective excitation mode in  $\text{Pr}_{0.7}\text{Ca}_{0.3}\text{MnO}_3$  by using THz time-domain spectroscopy *Phys. Rev. B* **66** 024401
- [12] Liu X, Jin Z, Cheng Z, Lin X, Balakrishnan G and Ma G 2017 Terahertz spectra revealing the collective excitation mode in charge-density-wave single crystal  $\text{LuFe}_2\text{O}_4$  *Phys. Status Solidi* **11** 1700177
- [13] Rana R, Pandey P, Phanindra V E, Prabhu S S and Rana D S 2018 Terahertz spectroscopic evidence of low-energy excitations in  $\text{NdNiO}_3$  *Phys. Rev. B* **97** 045123
- [14] Rana R, Awari N, Pandey P, Singh A, Prabhu S S and Rana D S 2013 Erratum: charge-density wave condensate in charge-ordered manganites: impact of ferromagnetic order and spin-glass disorder *J. Phys.: Condens. Matter* **25** 129501
- [15] Pandey P, Awari N, Rana R, Singh A, Prabhu S S and Rana D S 2012 Charge density waves condensate as measure of charge order and disorder in  $\text{Eu}_{1-x}\text{Sr}_x\text{MnO}_3$  ( $x = 0.50, 0.58$ ) manganites *Appl. Phys. Lett.* **100** 062408
- [16] Kitano H, Inoue R, Maeda A, Motoyama N, Takaba M, Kojima K *et al* 2001 Microwave and millimeter wave spectroscopy in the slightly hole-doped ladders of  $\text{Sr}_{14}\text{Cu}_{24}\text{O}_{41}$  in the slightly hole-doped ladders of  $\text{Sr}_{14}\text{Cu}_{24}\text{O}_{41}$  *Europhys. Lett.* **56** 434
- [17] Gorshunov B, Haas P, Room T, Dressel M, Vuletić T, Korinhamzi B *et al* 2002 Charge-density wave formation in  $\text{Sr}_{14-x}\text{Ca}_x\text{Cu}_{24}\text{O}_{41}$  *Phys. Rev. B* **66** 060508
- [18] Blumberg G, Littlewood P, Gozar A, Dennis B S, Motoyama N, Eisaki H *et al* 1999 Sliding density wave in  $\text{Sr}_{14}\text{Cu}_{24}\text{O}_{41}$  ladder compounds *Science* **297** 584
- [19] Thorsmølle V K, Homes C C, Gozar A, Blumberg G, Van Mechelen J L M, Kuzmenko A B *et al* 2012 Phonon energy gaps in the charged incommensurate planes of the spin-ladder  $\text{Sr}_{14}\text{Cu}_{24}\text{O}_{41}$  compound by Raman and infrared spectroscopy *Phys. Rev. Lett.* **108** 217401
- [20] Bag R, Hazra S, Kini R N and Singh S 2019 Excess specific heat from the gapped sliding phonon modes in the incommensurate composite crystal  $\text{Sr}_{14}\text{Cu}_{24}\text{O}_{41}$  *Phys. Rev. B* **99** 054305
- [21] Bag R, Karmakar K and Singh S 2017 Travelling-solvent floating-zone growth of the dilutely Co-doped spin-ladder compound  $\text{Sr}_{14}(\text{Cu}, \text{Co})_{24}\text{O}_{41}$  *J. Cryst. Growth* **458** 16–26
- [22] Hiroi Z, Amelinckx S, Van Tendeloo G and Kobayashi N 2002 Microscopic origin of dimerization in the  $\text{CuO}_2$  chains in  $\text{Sr}_{14}\text{Cu}_{24}\text{O}_{41}$  *Phys. Rev. B* **54** 15849–55
- [23] Vaisakh C P, Mascarenhas A and Kini R N 2015 THz generation mechanisms in the semiconductor alloy,  $\text{GaAs}_{1-x}\text{Bi}_x$  *J. Appl. Phys.* **118** 165702
- [24] Gozar A, Blumberg G, Littlewood P B, Dennis B S, Motoyama N, Eisaki H *et al* 2003 Collective density-wave excitations in two-leg  $\text{Sr}_{14-x}\text{Ca}_x\text{Cu}_{24}\text{O}_{41}$  ladders frequency (GHz) *Phys. Rev. Lett.* **91** 087401
- [25] Vuletić T, Ivek T, Korin-Hamzić B, Tomić S, Gorshunov B, Haas P *et al* 2005 Anisotropic charge modulation in ladder planes of  $\text{Sr}_{14-x}\text{Ca}_x\text{Cu}_{24}\text{O}_{41}$  *Phys. Rev. B* **71** 012508
- [26] Murakami H, Kiwa T, Kida N, Tonouchi M, Uchiyama T, Iguchi I *et al* 2002 Partial and macroscopic phase coherences in an underdoped  $\text{Bi}_2\text{Sr}_2\text{CaCu}_2\text{O}_{8+\delta}$  thin film *Europhys. Lett.* **60** 288–94
- [27] Romero D, Liu S, Drew H D and Ploog K 1990 Observation of a metallic impurity band in n-type GaAs *Phys. Rev. B* **42** 3179–82
- [28] Sirenko A A, Marsik P, Bernhard C, Stanislavchuk T N, Kiryukhin V and Cheong S W 2019 Terahertz vortex beam as a spectroscopic probe of magnetic excitations *Phys. Rev. Lett.* **122** 237401
- [29] Nucara A, Maselli P, Calvani P, Sopracase R, Ortolani M, Gruener G *et al* 2008 Observation of charge-density-wave excitations in manganites *Phys. Rev. Lett.* **101** 066407
- [30] Kim T W, Donovan S, Griener G and Philipp P 1991 Charge-density-wave dynamics in  $(\text{Ta}_{1-x}\text{Nb}_x\text{Se}_4)_2\text{I}$  alloys *Phys. Rev. B* **43** 6315
- [31] Fukaya R, Okimoto Y, Kunitomo M, Onda K, Ishikawa T, Koshihara S *et al* 2015 Ultrafast electronic state conversion at room temperature utilizing hidden state in cuprate ladder system *Nat. Commun.* **6** 8519
- [32] Hazra S *et al* 2020 unpublished.
- [33] Thomson M D, Rabia K, Meng F, Bykov M, Van Smaalen S and Roskos H G 2017 Phase-channel dynamics reveal the role of impurities and screening in a quasi-one-dimensional charge-density wave system *Sci. Rep.* **7** 1–9
- [34] Takada S, Wong K Y M and Holstein T 1985 Damping of charge-density-wave motion *Phys. Rev. B* **32** 4639–52
- [35] Richard J and Chen J 1993 Damping of charge-density waves in  $\text{NbSe}_3$  *Solid State Commun.* **86** 485–8
- [36] Rusydi A, Abbamonte P, Eisaki H, Fujimaki Y, Blumberg G, Uchida S *et al* 2006 Quantum melting of the hole crystal in the spin ladder of  $\text{Sr}_{14-x}\text{Ca}_x\text{Cu}_{24}\text{O}_{41}$  *Phys. Rev. Lett.* **97** 016403
- [37] Bag R, Karmakar K, Dhar S and Tripathi M 2019 Effect of impurities on the long-distance and Zhang—rice dimers in the quantum *J. Phys.: Condens. Matter* **31** 035801
- [38] Isobe M, Ohta T, Onoda M, Izumi F, Nakano S, Li J *et al* 1998 Structural and electrical properties under high pressure for the superconducting spin-ladder system *Phys. Rev. B* **57** 613–21
- [39] Tsuchiizu M and Suzumura Y 2004 Charge-density-wave formation in the doped two-leg extended Hubbard ladder *J. Phys. Soc. Japan* **73** 804–7